ISBN: 978-3-95450-241-7 ISSN: 2673-5350 doi:10.18429/JACoW-IBIC2022-TUP18

HIGH-RESOLUTION INTERFEROMETRIC BEAM-SIZE MONITOR FOR LOW-INTENSITY BEAMS

B. Alberdi-Esuain*,[1], J.-G. Hwang, T. Kamps[1]
Helmholtz-Zentrum Berlin für Materialien und Energie, Berlin, Germany
[1]also at Humboldt Universität zu Berlin, Berlin, Germany

Abstract

Plasma-based accelerator technology is reaching a mature state, where applications of the beam for medical sciences, imaging, or as an injector for a future large-scale accelerator-driven light source become feasible. Particularly, the requirements for beam injection into a storage-ring-based light source are very strict with regards to beam quality and reliability. A non-invasive diagnostics greatly helps to reduce the commissioning time of the machine. We present a device suitable for online, non-destructive monitoring of the transverse spot size of the injected beam. In order to measure lateral beam sizes with a few-µm resolution, the technique uses an interferometric regime of coherent synchrotron radiation that is enabled by a sub-femtosecond short bunch-length. Simulations of the photon flux and the retrieval of the beam spot-size are performed for different bandwidth filters in order to define the bandwidth acceptance. Results show the potential of the proposed system that achieves precise retrieval of the complex degree of coherence at an extremely low photon intensity similar to those expected towards the plasma-acceleration injectors.

INTRODUCTION

In the last years, the laser plasma-accelerator technology has advanced enough to produce charged-particle beams stably with ultra-low-emittances in 6D phase-space [1]. These achievements have enabled the application of plasma-accelerator technology for low-energy and high-quality injectors. Recent research evidence that the repetition rate of such a technique is not limited by plasma recovery time in the plasma cell, so it is promising to reach MHz repetition [2]. This feature opens a possibility to supersede the state-of-the-art injectors. Currently, there is an ongoing global effort aimed towards designing a compact plasma-wakefield accelerator as an injector for future large-scale accelerator-driven light sources such as Athena$_e$ [3] or cSTART [4] for injection into ring-based light-sources, high-average-power plasma wakefield research with FLASHForward [5] or projects to apply this technology for free electron lasers directly [1]. These novel injectors can generate electron beams with an extremely low-emittance on the order of $\gamma\epsilon_{x,y} = 0.05\,\text{mm}\cdot\text{mrad}$ for pC to sub-pC bunch charges. The important beam parameters of these facilities are listed in Table 1.

Diagnostics techniques are following the steps forward of laser-plasma accelerators closely, particularly the non-invasive spot-size measurement which inherently gives the beam emittance information. The characterisation of the electron distribution with the sufficient resolution is challenging due to the extremely small beam emittances and intensities in plasma-wakefield accelerators. Techniques that employ scintillation screens are widely used for similar beam conditions [6], but this deteriorates the beam quality noticeably or even it causes beam loss in the following section. On the other hand, synchrotron-radiation-based monitors is inadequate since light intensity by incoherent synchrotron radiation (ISR) is insufficient owing to the low electron intensity. However, the key feature of the laser-wakefield accelerators, temporally short bunch enables the arising of coherent synchrotron radiation (CSR) in the visible region, which enhances the photon flux significantly in a bending magnet. The photon flux by CSR provides sufficient intensity to place an interferometric beam size monitor (IBSM) which measures the lateral distribution of electrons by the spatial coherency of the interference pattern in the detector [7]. The use of the diffraction regime enhances the spatial resolution by two orders of magnitude, reaching µm-resolutions [8] and this has been applied to many storage-ring-based light sources [9–11]. By extension, we have designed and demonstrated the high-resolution IBSM for extreme beam conditions [12]. However, the detailed aspects of the bandwidth acceptance and beam spot-size retrieval are not fully discussed in the paper. Hence, numerical simulations for investigating the effect of bandwidth and for estimating the propagation of this error to the beam-size retrieval are explained. A scheme of the working principle of our design can be seen in Fig. 1.

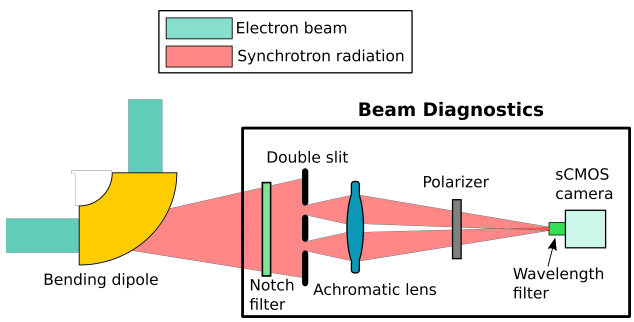

Figure 1: Schematic layout of the interferometry beam size monitor (IBSM) with a scientific complementary metal–oxide–semiconductor (sCMOS) camera for a plasma-wakefield accelerator.

* benat.alberdi_esuain@helmholtz-berlin.de

ISBN: 978-3-95450-241-7 ISSN: 2673-5350 doi:10.18429/JACoW-IBIC2022-TUP18

Table 1: Major Beam Parameters of Research Projects for a Plasma-wakefield Acceleration-based Injector Relevant for Our Case Study

	Energy (MeV)	$\gamma\epsilon$ (mm·mrad)	Bunch charge (pC)	Bunch length (fs)	Beam size at $\beta_{x,y}$=1 m (μm)
Athena$_e$ [3]	200	0.05	0.38-2.77	0.2-0.62	11
cSTART [4]	50	≤3	27.5	≤10	174
Shanghai LWFA [1]	490	≤3	50	/	15

METHODS

Double Slit Interference for 2D Gaussian Beams

The intensity distribution of interference fringes generated by a double-slit is found by using the basic theory of spatial coherence of light and the van Cittert-Zernike theorem which explains that the Fourier transform of the intensity distribution function of a distant, incoherent source is equal to its complex degree of spatial coherence (also known as interferometric visibility) under certain conditions. Assuming a Gaussian distribution of the source, the intensity distribution of the photons at the screen for a horizontal double slit can be presented for monochromatic light as

$$I(x,y) = I_0 + (I_1 + I_2)\,\mathrm{sinc}^2\left(\frac{\pi w_x x}{\lambda f}\right)\mathrm{sinc}^2\left(\frac{\pi w_y y}{\lambda f}\right)\cdot \left[1 + |\gamma_{12}|\cos\left(\frac{2\pi D_x x}{\lambda f} + \phi\right)\right], \quad (1)$$

where I_1 and I_2 are the photon intensity at two holes, respectively, w_x and w_y are the slit opening in horizontal and vertical directions, and γ_{12} is the visibility (complex degree of spatial coherence), f is the focal length of the objective lens, D_x is the slit separation, ϕ represents the phase differences between the two incident waves, and I_0 denotes the constant offset preset the value for a detector to compensate for negative values owing to random noise. For a Gaussian distributed source, the absolute value of the complex degree of coherence can furthermore be simplified as

$$\sigma_x = \frac{\lambda L}{\pi D_x}\sqrt{\frac{1}{2}\ln\frac{1}{|\gamma_{12}|}}, \quad (2)$$

where σ_x is the rms horizontal beam size and L is the distance from the source point to the slit. This relation allows quantifying the absolute beam size directly.

Operational Limit and Bandwidth Acceptance

In the previous study, it has proven that that the operating limit of the IBSM technique using the state-of-the-art single-photon camera is about 5 photons/pixel at the peak, which corresponds to a S/N ratio of about 4. This is equivalent to a total flux of 2×10^4 photons/s. The numerical simulation includes photon shot-noise which is caused by statistical quantum fluctuations and can be modeled by a Poisson process. However, the IBSM monitor requires primarily the obstacles such as a double slit for inducing diffraction generation, a polarization filter for rejecting the π-polarization component, and a wavelength filter for generating quasi-monochromatic light, which reduces the number of photons by two orders of magnitudes. It is generally not suitable for low flux beams which is the case for Athena$_e$ and cSTART projects. The photon flux can be escalated by widening the bandwidth of the filter and also can be enhanced by CSR generated by a short bunch. To estimate the photon flux by ISR and CSR for two cases of the plasma-wakefield accelerator, numerical simulations are performed using SPECTRA code [13] with beam parameters of Athena$_e$ and cSTART listed in Table 1. A magnetic field of 0.85 T in the bending magnet is used for the simulations and obstacles such as the optical wavelength filter and a double-slit with a slit opening of $3 \times 3\,\mathrm{mm}^2$ is included. The results are shown in Fig. 2.

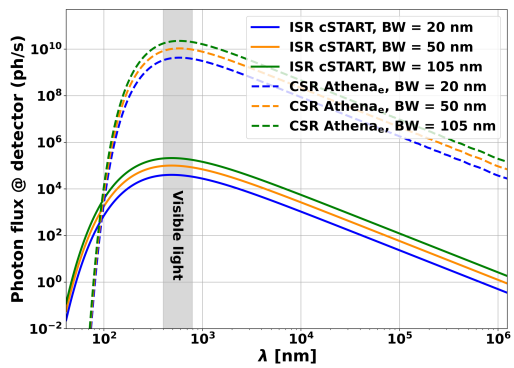

Figure 2: Photon flux at the detector for Athena$_e$ and cSTART beam parameters from Table 1 with various bandwidths. The photon flux by CSR shown here is calculated with the lower case of the bunch charge (0.38 pC) in Athena$_e$.

Taking the diminution of photon flux by the obstacles into account, the photon flux by ISR at the detector is 3.4×10^3 photons/s for the Athena$_e$ and 2.9×10^4 photons/s for cSTART at a bandwidth of 100 nm. Despite the photon flux of ISR for Athena$_e$ can not reach the operating limit, $\sim 2 \times 10^4$ photons/s, defined by the numerical simulation with the total noise and quantum efficiency of the camera, the photon flux by CSR overwhelms the limit easily which evidences that a narrow filter can be used. However, the photon flux by ISR for cSTART can overcome the operating limit by expanding the bandwidth of the filer. The wider the bandwidth of the filter, the greater the number of photons in the detector, but the dilution of the visibility caused by phase differences of non-monochromatic light becomes more severe, resulting in inaccurate beam size measurements since

ISBN: 978-3-95450-241-7 ISSN: 2673-5350 doi:10.18429/JACoW-IBIC2022-TUP18

the effect of a finite bandwidth is not accounted in Eq. (1). In order to quantify the effect of the bandwidth in the beam size determination, numerical simulations are performed based on Monte-Carlo method. Two-dimensional coordinates of photons at the detector were generated for a specified photon intensity with a random uniform distribution of the wavelength and probability density function that follows Eq. (1). Then, an artificial image was generated by counting the number of particles within a finite size of a pixel and adding Poisson noise onto each pixel. Each image is first projected into the slit axis and is analyzed based on fitting with an analytical formula. The projections simulated with various bandwidths at a visibility value of 0.5 are shown in Fig. 3. It is clear that the fringes are not significantly

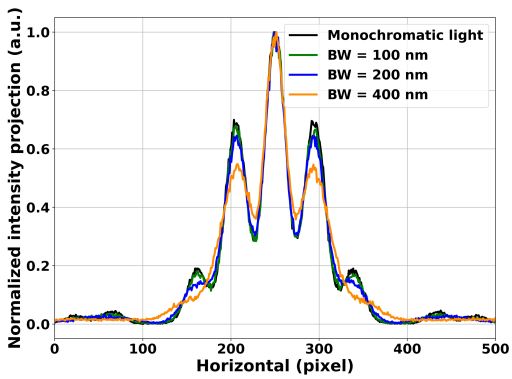

Figure 3: Simulated interference pattern at the detector for a visibility value of $|\gamma_{1,2}| = 0.5$ with various bandwidths. The simulations have been performed with a flux of 1×10^5 photon/s at the detector.

distorted for a bandwidth below 100 nm, but the distortion is non-negligible for larger bandwidths.

In order to estimate the statistical fluctuation of the visibility retrieval, the analysis is repeated for fifty different images generated for each intensity at various visibility values. The visibility can be adjusted by changing the experimental set-up such as magnitudes of L, λ and D to get a desired visibility for a given spot size. Therefore, the calculation has been performed with various visibilities. Fig. 4 shows that the retrieved visibility is underestimated for large visibilities and overestimated for the lowest ones. The error is minimized around visibility of 0.5. Therefore, to obtain the reliability of the monitor, the visibility is necessary to be tailored to the intermediate values by changing the experimental set-up. The measurement accuracy is improved with photon flux, which can be enhanced by widening the bandwidth of a wavelength filter. An increasing bandwidth decreases the visibility retrieval accuracy and, as a consequence, the beam-size resolution.

In order to estimate the measurement error in the beam size determination quantitatively, the relative error of the beam size calculation as a function of the bandwidth at various visbilities are computed. The error transfer from relative visibility retrieval error($|\Delta\gamma/\gamma|$) to spatial resolution ($\Delta\sigma$) is calculated according to the following equation: $\Delta\sigma = \lambda L / \left(2\pi D\sqrt{2\ln|1/\gamma|}\right) \times |\Delta\gamma/\gamma|$. The result is shown in Fig. 5.

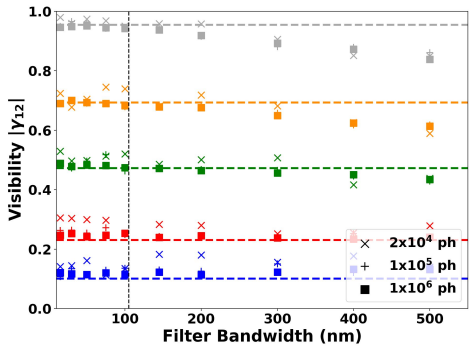

Figure 4: The retrived visibility as a function of the bandwidth at different photon fluxes and visibility (in dashed horizontal lines).

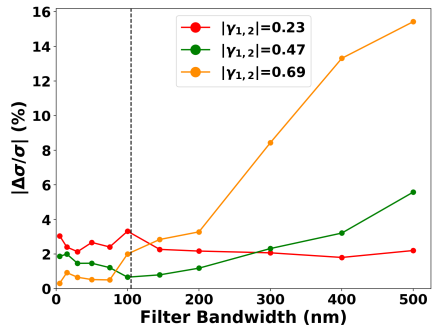

Figure 5: Relative error of the retrieved beam spot-size as a function of the bandwidth at intermediate $|\gamma_{1,2}|$ values, which depend on the beam spot-size and the experimental set-up.

For the intermediate visibility values of 0.47 and 0.69 with the chosen bandwidth of 105 nm for our device, the error of the beam size measurement remains below a few percentages. It also indicates that the smaller visibility has much less error when the bandwidth is increased because the local minima of the interference fringe raise for the lower visibility, resulting in immune to the statistical error that has been introduced by the bandwidth. The error of the visibility retrieval is smaller than 3.6% at the operating limit with a bandwidth of 105 nm. This results in a spatial resolution of fewer than 1 µm since the beam size is in the order of tens of micrometers due to the extremely low emittance. It can be also improved significantly by narrowing the bandwidth of the wavelength filter. This shows that as long as the photon flux is kept over the operating limit, a narrow bandwidth acceptance is preferred.

ISBN: 978-3-95450-241-7 ISSN: 2673-5350 doi:10.18429/JACoW-IBIC2022-TUP18

CONCLUSIONS

Plasma-wakefield accelerators produce a high quality beams with a low average beam-current which results in a lack of the photon intensity by synchrotron radiation, so this feature calls for research and development for high spatial-resolution diagnostics that can be operated at a low photon intensity. For the Athena$_e$ project, the beams have a temporal size of sub-femtosecond which is comparable to or even shorter than the wavelength of visible light, producing intense CSR. This enables the implementation of the interferometric technique that can achieve a few-μm spatial resolution. However, for the beams in cSTART that have a bunch length longer than the wavelength, it demands a broad filter to achieve the photon flux greater than the operating limit. Therefore, we have studied the effects of the bandwidth in the beam-size retrieval error. The statistical error of the IBSM by the quasi-monochromatic light is investigated for estimating the measurement accuracy of an absolute lateral size at the extreme beam condition. The error of the visibility retrieval is less than 3.6% at the operating limit with a bandwidth of 105 nm for a cSTART beam condition. This results in a spatial resolution of fewer than 1 μm.

REFERENCES

[1] W. Wang *et al.*, "Free-electron lasing at 27 nanometres based on a laser wakefield accelerator", *Nature*, vol. 595, pp. 516–520, 2021. doi:10.1038/s41586-021-03678-x

[2] R. D'Arcy *et al.*, "Recovery time of a plasma-wakefield accelerator", *Nature*, vol. 603, pp. 58–62, 2022. doi:10.1038/s41586-021-04348-8

[3] B. Marchetti *et al.*, "Technical Design Considerations About the SINBAD-ARES Linac", in *Proc. IPAC'16*, Busan, Korea, May 2016, pp. 112–114. doi:10.18429/JACoW-IPAC2016-MOPMB015

[4] B. Härer *et al.*, "Non-Linear Features of the cSTART Project", in *Proc. IPAC'19*, Melbourne, Australia, May 2019, pp. 1437–1440. doi:10.18429/JACoW-IPAC2019-TUPGW020

[5] R. D'Arcy *et al.*, "FLASHForward: plasma wakefield accelerator science for high-average-power applications", *Philos. Trans. R. Soc. London, Ser. A*, vol. 377, 2019. doi:10.1098/rsta.2018.0392

[6] M. C. Downer, R. Zgadzaj, A. Debus, U. Schramm, and M. C. Kaluza, "Diagnostics for plasma-based electron accelerators", *Rev. Mod. Phys.*, vol. 90, p. 035002, 2018. doi:10.1103/RevModPhys.90.035002

[7] T. Mitsuhashi, "Beam Profile and Size Measurement by SR Interferometers", in *Beam Measurement: Proceedings of the Joint US-CERN-Japan-Russia School on Particle Accelerators*, Editors S-i. Kurokawa, S.Y. Lee, E. Perevedentsev and S. Turner, p. 399–427, World Scientific, Singapore, 1999.

[8] T. Naito and T. Mitsuhashi, "Very small beam-size measurement by a reflective synchrotron radiation interferometer", *Phys. Rev. ST Accel. Beams*, vol. 9, p. 122802, 2006. doi:10.1103/PhysRevSTAB.9.122802

[9] C. Kim *et al.*, "Two-dimensional SR interferometer for PLS-II", *J. Korean Phys. Soc.*, vol. 58, pp. 725–729, 2011. doi:10.3938/jkps.58.725

[10] L. Torino and U. Iriso, "Transverse beam profile reconstruction using synchrotron radiation interferometry", *Phys. Rev. ST Accel. Beams*, vol. 19, p. 122801, 2016. doi:10.1103/PhysRevAccelBeams.19.122801

[11] M. Koopmans, P. Goslawski, J. G. Hwang, M. Ries, M. Ruprecht, and A. Schaelicke, "Status of a Double Slit Interferometer for Transverse Beam Size Measurements at BESSY II", in *Proc. IPAC'17*, Copenhagen, Denmark, May 2017, pp. 149–152. doi:10.18429/JACoW-IPAC2017-MOPAB032

[12] J.-G. Hwang *et al.*, "Monitoring the size of low-intensity beams at plasma-wakefield accelerators using high-resolution interferometry", *Commun. Phys.*, vol. 4, 2021. doi:10.1038/s42005-021-00717-x

[13] T. Tanaka and H. Kitamura, "SPECTRA: a synchrotron radiation calculation Code", *J. Synchrotron Radiat.*, vol. 8, pp. 1221–1228, 2001. doi:10.1107/S090904950101425X